Research Article

BIOMEDICAL Journal of Scientific & Technical Research

ISSN: 2574 -1241

DOI: 10.26717/BJSTR.2020.24.004054

Quantification of Entire Tumor Vascular Normalization in Response to A VEGF Inhibitor

Chung-Wein Lee[1],*, Jian Wang[2], Todd Christopher[1], Eric Su[1], Kuldeep Neote[1], Michael Westmore[1]

[1]*Lilly Research Laboratories, Eli Lilly and Company, Indianapolis, USA*

[2]*Wyeth Pharmaceuticals, Collegeville, PA*

***Corresponding author:** Chung-Wein Lee, Eli Lilly and Company, Lilly Research Laboratories, Indianapolis, Indiana 46285, USA

ARTICLE INFO

Received: December 14, 2019

Published: January 09, 2020

Citation: Chung-Wein Lee, Jian Wang, Todd Christopher, Eric Su, Kuldeep Neote, Michael Westmore. Quantification of Entire Tumor Vascular Normalization in Response to A VEGF Inhibitor. Biomed J Sci & Tech Res 24(3)-2020. BJSTR. MS.ID.004054.

Abbreviations: GIST: Gastrointestinal Stromal Tumors; VEGF: Vascular Endothelial Growth Factor

Abstract

A comprehensive vascular analysis is crucial for extending our understanding of angiogenesis and to evaluate the efficacy of anti-angiogenic therapies in cancer. No analysis based upon the entire tumor vasculature has been established. We have developed several morphological imaging markers to analyze entire vascular structures from a human non-small cell lung carcinoma subcutaneous xenograft using micro-computed tomography. The imaging markers aim to condense complicated three-dimensional vascular structures to simple numbers and tables. The design of the imaging markers was motivated by the physiology and function of vascular systems. We tested the markers on 30 mice in four groups: one-week and two-week vehicle groups; one-week and two-week Stent administration groups. Vascular normalization after anti-angiogenic treatment was quantified. The imaging markers verified that micro-vessel sprouting followed by dilation and large-vessel segment enlargement occurred in tumor progression. This methodology can assist researchers to objectively and quantitatively validate the efficacy of anti-angiogenic compounds and combinational therapies..

Keywords: Imaging Markers; Contrast Enhanced Micro-Computed Tomography; Vasculature Normalization; Tumor Angiogenesis; Sutent/Sunitinib Malate

Introduction

Angiogenesis is associated with numerous diseases and physiological processes in the body [1-3]. Recent discoveries also elucidate the connection and common mechanisms between angiogenesis and other networks [3-6]. Tumor-induced pathological angiogenesis dictates the growth of many solid tumors. Uncontrolled tumor cells require excessive nutrient and oxygen supply to survive and metastasize [7]. When normal physiological vascular networks around tumors cannot compensate for the demand, unregulated growth factors from tumor cells trigger abnormal nascent vessel sprouting and irregular pruning leading to over vascularization. The immature vessel networks are heterogeneous and leaky, resulting in low delivery efficiency to surrounding tissues compared to normal vascular structures [8].

Targeting tumor angiogenesis as cancer therapy was proposed by Folkman in 1971. The Vascular Endothelial Growth Factor (VEGF) family and receptors have proved to be essential to physiological and pathological angiogenesis [9]. VEGF administration also induces lymph angiogenesis [10-13]. Clinical studies showed that anti-angiogenic therapy combined with other cancer therapies (such as cytotoxic drugs and radiation therapy) yielded better survival rates than monotherapy [13-16]. The vascular normalization hypothesis supplies an explanation of why combinational therapy results in better overall survival than monotherapy. It also suggests that the degree of vascular normalization due to anti-angiogenic therapy may dictate the efficacy of the following cytotoxic therapy. In order to yield better survival rates from the combinational therapy paradigm, quantification of vascular morphology during the anti-angiogenic regimen is critical [16,17].

We used Sutent in this study as an anti-angiogenic compound to quantify the vascular normalization in response to two regimens. Sutent (SU11248, sunitinib malate, Pfizer, Inc., New York, NY, USA) is a small-molecule, multi-target tyrosine kinase inhibitor with

high affinity for the PDGF and VEGF receptors [18]. Dual delivery of VEGF and PDGF-BB returned more mature vessel formation than either single growth factor. Sutent has demonstrated anti-tumor activity and inhibition of angiogenesis in clinical trials [19,20]. It was approved by the FDA in January of 2006 to treat renal cell carcinoma and imatigib-resistant Gastrointestinal Stromal Tumors (GIST). Imaging technology has advanced significantly over the last decade for drug research and clinical diagnoses. Various imaging modalities with proper imaging analysis methods have been utilized to reveal the function and anatomy of vascular structures in differing spatial and temporal resolutions [21,22]. Contrast-enhanced μ CT is able to reconstruct three-dimensional (3-D) vascular structures with resolution of a few microns. In this study, the isotropic voxel dimension of all images in the vehicle and the treated groups was 16 μ m (Figure 1A & 1B).

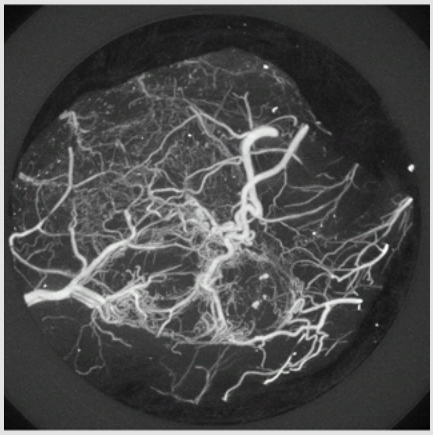

Figure 1A: Maximum Intensity Projection (MIP) of 3-D tumor-induced vasculature. A two-week 3-D tumor vasculature MIP image illustrates the excessive abnormal sprouting and tortuosity in the entire tumor. The 3-D vascular structure was acquired by μ CT imaging modality with contrast agent injection. The isotropic voxel size of 3-D vasculature is 16 μ m.

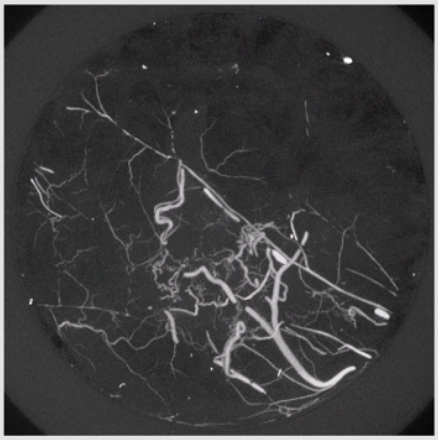

Figure 1B: MIP demonstration of vascular remodeling in response to two-week Sutent treatment. A significant qualitative vascular structure alteration compared to a two-week vehicle is easily recognized. Entire vascular normalization in the tumor due to the Sutent compound (less sprouting, less tortuosity) is observed.

This study aimed to develop imaging parameters to objectively quantify entire 3-D vascular configurations and to differentiate the vascular remodeling due to treatment with anti-angiogenic agents. The hope is that the imaging markers can differentiate vascular evolution during tumor progression and during treatment with different anti-angiogenic therapies. The imaging markers can be used to characterize the response to anti-angiogenic therapies not only for cancer but also for other angiogenesis-related diseases into different aspects of vascular structure. Furthermore, correlation between the molecular interactions and entire vasculature morphological remodeling via imaging markers can be established.

Materials and Methods

Tumor Xenograft

Female CB-17 SCID mice, 6-7 weeks old, (Charles River, Wilmington, MA) were acclimated for one week prior to the study. The human alveolar epithelial cell carcinoma line A549 (ATCC, Manassas, VA) was established in culture and cells were mixed with Matrigel in a 1:1 ratio. Each mouse was implanted with 107 cells subcutaneously on the back. Treatment began 7 days after inoculation, when tumor volumes were 100-150 mm^3. Animals were randomized into four groups of 8 mice each, based on tumor size. The mice in the treated groups were given Sutent orally twice a day (20mg/kg, 0.1ml/mouse); the mice in the vehicle groups were given 1% NaCMC / 0.25%Tween80 / 0.05% antifoam (0.1ml/mouse). Animal perfusion was performed the day after the last dose (either day 8 or day 15).

Contrast Agent Perfusion

Nude mice carrying intradermal tumor xenografts of A549 human lung cancer cells were used in this experiment. The mice were anesthetized with 3% isoflurane inhalation and local hair was removed with Nair hair remover. The animals were placed on a drainage tray and the core temperature was maintained between 37°C and 39°C. Thoracotomy was performed, and a 23-g needle was immediately inserted into the left ventricle, while the right atrium was cut for drainage. Systemic perfusion was performed with a pre-warmed vasodilation buffer (4 mg papaverine and 1 gm adenosine in 1000 ml of PBS) under 90-110 mmHg pressure for 5 minutes until the outlet became clear. 4.75ml of fresh prepared Microfil working solution, consisting of 2ml of MV-122 (Yellow), 2.5ml of MV-Diluent and 0.25ml of MV-Curing Agent (Flow Tech, Inc. Carver, MA), was injected into the left ventricle under constant pressure (130-150mmHg). The excess Microfil spilled from the right atrium opening. After being held at room temperature for at least 90 minutes to allow the contrast agent to solidify, the animal bodies were fixed in 70% alcohol for CT scanning.

Micro-CT Scanning

Each tumor xenograft with surrounding tissue was cut off and placed in a 15-mm tube (without medium) and scanned with the explore Locus SP Micro-CT Scanner (GE Healthcare). The scan parameters used included a tube voltage of 80 kVp, 400 views acquired with an angle increment of 0.5o, a total tube current-time

product of 110 mAs, 0.020" aluminum filtration, and a 33-minute scan time. Calibration was performed with air-, water-, and bone-mimicking materials in a calibration phantom. Bright and dark fields were collected for correction of the acquired images. The two-dimensional projections were reconstructed into a 3D volume with 16- μ m isotropic voxels using the explore Reconstruction Utility.

Imaging Analysis

The raw 16-bit volumetric tumor images were loaded into the workspace of Analyze 7.0 (Mayo Clinic, Rochester MN) in unsigned 8-bit format. High spatial-frequency noise was removed by using a 3x3x3 low-pass filter. The 3-D vascular structure extraction was completed using the Tree Analysis module of Analyze 7.0 [23]. The intensity threshold ranged from 130 to the highest voxel intensity. The shortest skeleton branch was set to be either 4 or 7, while the minimum tree length was 25. Commonly, more than one tree was generated. The first tree, however, was extensive enough to represent the whole vascular structure. We tested the performance of the imaging markers based upon one tree and all the trees, and the outcomes were close. In the study, we considered all trees if the computation time for the imaging marker calculations was not demanding. A single vessel in this study was defined to be from the root to an end node of the tree. Accordingly, the number of end nodes defined the number of vessels of a vascular tree. Segments of a vessel were defined between two branch points or between a branch point and an end node (**Supplementary Figure 1**). All imaging marker algorithms were programmed in MATLAB (MathWorks, Inc.). The definition of the imaging markers is in the **Supplementary Methods** online. We applied identical algorithms to analyze all 30 animals in this study. JMP 6 (SAS Institute Inc.) was the statistics software to calculate the significance of the imaging markers in the two groups.

Results

Vessel Length Distribution of Vehicle and Sutent-treated Groups

Excessive vessel sprouting from a pre-existing vascular network is a vital hallmark of angiogenesis in tumors. Vessel length calculation from a 3-D vasculature image is a direct approach to quantify angiogenesis. Our vessel length imaging marker measures the normalized vessel length distribution, defined as the distance from the root of a vascular tree to the end nodes (**Supplementary Figure 1**, **Supplementary Methods**). In this study, the maximum vessel length of the one-week and two-week treated groups was estimated to be about 100 mm, which was significantly less than the 180 mm maximum vessel length of the one-week vehicle group and the 240 mm maximum vessel length of the two-week vehicle group (Figure 2). The treated groups had a higher population of short vessels, while the vehicle groups had a higher population of long vessels. 81 percent of the vessels in the one-week treated group measured less than 50 mm; meanwhile, 61 percent of the vessels in the two-week treated group were found to be less than 50 mm. In contrast to the treated groups, the one-week vehicle group showed 43 percent of the vessel population to be less than 50 mm, and the two-week vehicle group revealed only 23 percent under 50 mm. This quantitatively proved that Sutent inhibited new vessel sprouting in the entire 3-D vascular tree. In consideration of the angiogenesis comparison between the two control groups, approximately 4.5 percent of the vessels in the one-week vehicle group had lengths longer than 150 mm; more than 15 percent of the vessels in the two-week vehicle group were extended beyond the same threshold. This indicated that tumor-induced angiogenesis progressed from week one to week two.

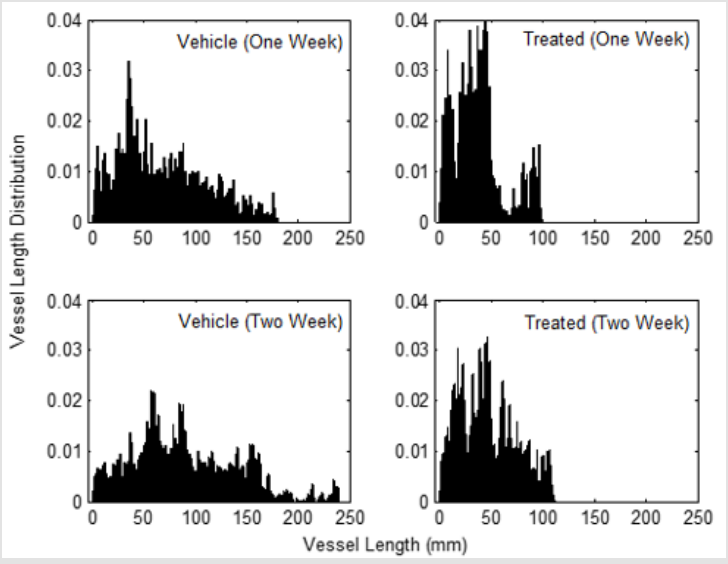

Figure 2: Vessel length histograms of vehicle and Sutent-treated groups. Each histogram is normalized by the total vessel number of the group. The bin size of the histogram is 1.6mm. The maximum vessel length for the two-week vehicle group exceeded 250mm; however, the population of vessels with lengths over 240mm is limited.

Vessel Tortuosity Distribution

During the progression of the tumor, the vascular network becomes chaotic and tortuous. Direct or indirect anti-angiogenic therapies prune immature vessels to reduce the vascular tortuosity. The normalized network should deliver drugs and nutrients to tumor cells with better efficiency. We applied a simple formula to determine the modification of the entire vascular tortuosity distribution during tumor growth and the response to the Sutent regimens (**Supplemental Figure 1**, **Supplementary Methods**). More low tortuosity vessels were found in the Sutent-treated groups than in the vehicle groups (Figure 3). In contrast, Figure 3 shows that the vehicle groups had a higher population of more tortuous vessels than the Sutent-treated groups. Table 1 lists the details of the tortuosity distributions in Figure 3 grouped into three domains (low tortuosity, high tortuosity, and ultra-high tortuosity). The vessels with tortuosity between 3 and 12 were categorized as low tortuosity; the vessels belonging to the high tortuosity domain had tortuosity between 13 and 70; the ultrahigh tortuosity domain contained the vessels with tortuosity beyond 71. The quantitative alteration of the tortuosity in the three domains was compared between groups (Table 1).

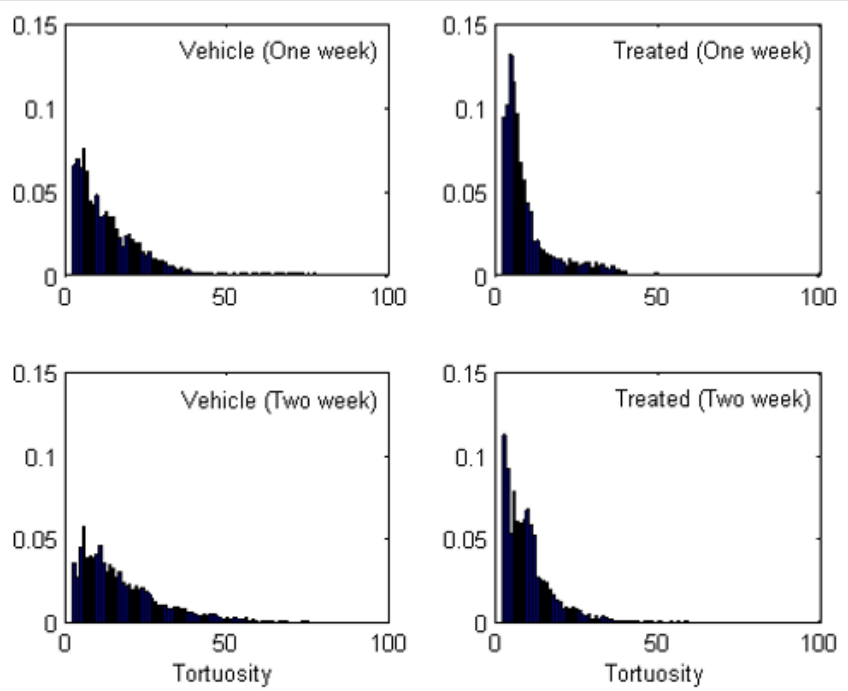

Figure 3: Vessel tortuosity histograms of vehicle and Sutent-treated groups. Tortuosity is a dimensionless parameter. The tortuosity histogram of a group is normalized by the total number of vessels from the group as with the vessel length histogram. The bin size of the tortuosity histogram is one.

Table 1: Low, high, ultrahigh vessel tortuosity population.

	Tortuosity (3:12)	Tortuosity (13:70)	Tortuosity > 70
Treated (One week)	0.765	0.235	0
Vehicle (One week)	0.542	0.441	0.017
Difference	0.224	-0.207	-0.017
Treated (Two week)	0.699	0.296	0.0051
Vehicle (Two week)	0.409	0.569	0.0221
Difference	0.291	-0.274	-0.017
Vehicle (One week)	0.542	0.441	0.017
Vehicle (Two week)	0.409	0.569	0.0221
Difference	0.133	-0.128	-0.0051
Treated (One week)	0.765	0.235	0
Treated (Two week)	0.699	0.296	0.0051
Difference	0.066	-0.061	-0.0051

More than 76 percent of the vessels in the one-week Sutent group were in the low tortuosity domain; in contrast, only 54 percent of the vessels in the one-week vehicle group were in the low tortuosity domain. In the week two Sutent and vehicle comparison, about 70 percent of Sutent-treated vessels were detected in the low tortuosity domain while only 41 percent of vehicle vessels belonged to the low tortuosity domain. This objective tortuosity marker provided unambiguous vascular normalization validation and quantification. The vessel population comparison of the two vehicle groups in the low and high tortuosity domains supported the observation from the vessel length marker that angiogenesis in the tumors advanced from week one to week two.

Vascular Volume Measurement

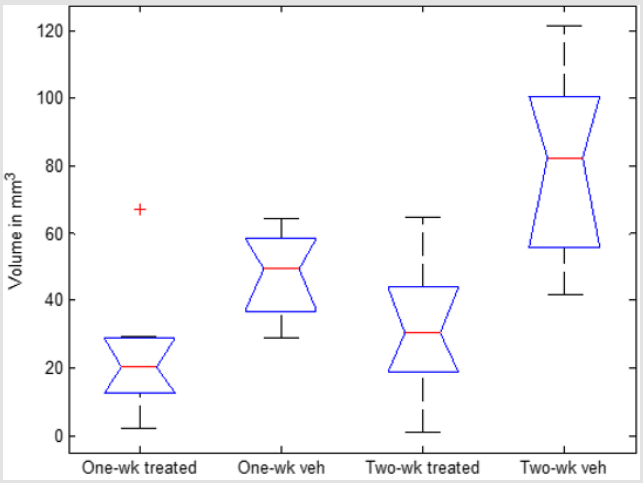

Figure 4A: Boxplot of vascular volume. Box and Whisker plots are used to calculate the median volume and variability of volume between samples. The median volume in mm^3 of a group is indicated by a red line. The lines at the top and bottom represent the upper and lower quartile values. Outliers of a grouped data are displayed by a Red cross. Notches in the plot are related to the variability. The samples whose notches do not overlap have different medians at a 95% confidence level.

The measurement of tumor volume incorporating the necrotic core has been used as an important prognostic parameter to indicate patient survival and response to cancer therapies [23-28]. Many tumor volume estimation methods have been proposed to increase sensitivity and accuracy in diagnoses [29]. Vascular volume is a direct scalar measurement of angiogenic sprouting activity. Here we calculated the whole 3-D vascular volume in the tumors (**Supplementary Methods**). The median volumes of the one-week vehicle group and one-week treated group were 49.4 and 20.4 mm^3 respectively (Figure 4A). In the week two comparison, the median vehicle-group volume was enlarged to 82.5 mm^3 while the median volume of the treated group shifted to 30.5 mm^3. Since the notch of vehicle and treated groups did not overlap, the median volume difference between vehicle and treated groups evaluated at the same time point should be above 95% confidence (Figure 4A). Although the two-week treated vascular volume was greater than the one-week treated group, the median volume ratio of the treated to the vehicle group at week two was less than the ratio at week one. The significant volume increase of the two-week vehicle group over the one-week vehicle group could be the consequence of both angiogenic sprouting and vessel dilation during tumor growth.

Micro-Vessel Lumen Surface Area

We designed a micro-vessel lumen surface area marker to investigate the change of lumen surface area between the vehicle and treated groups (**Supplementary Methods**). Three diameter thresholds were defined to evaluate the total lumen surface area contributed by vessel segments (**Supplementary Figure 1**) in a 3-D vascular structure with diameters less than the assigned threshold. This analysis also leads to the diameter distribution. Figure 4B displays the mean and standard deviation of lumen surface area using the three diameter thresholds (50 μ m, 70 μ m, and 107 μ m). The Sutent treated groups had smaller micro-vessel surface areas than their related vehicle groups under all thresholds. The lumen surface areas of the one-week treated group and the two-week treated group were comparable. We applied a pair-wise t-test to evaluate the significance of the lumen surface area differences between the two vehicle groups under the same thresholds (**Supplementary Notes**, Figure 4B). The average lumen surface areas using the 50 μ m and 70 μ m thresholds for the one-week vehicle group were less than those for the two-week vehicle group. The average lumen area for the one-week vehicle group using the 107 μ m threshold, however, became greater than that for the two-week vehicle group.

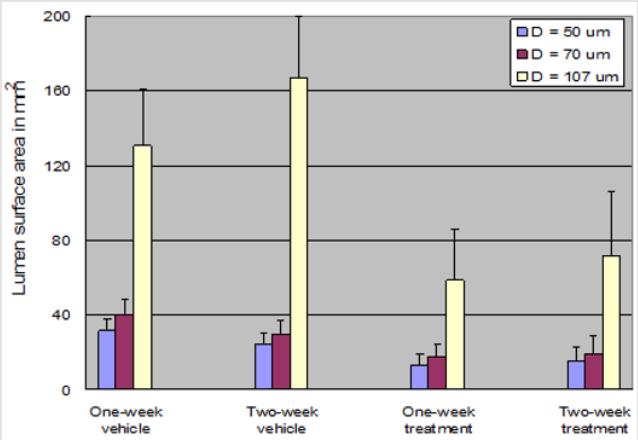

Figure 4B: Average micro-vessel lumen surface area. Column heights indicate the average micro-vessel area contributed from vessel segments with diameters less than thresholds of 50, 70, and 107 μ m. The error bars are the standard deviations of the groups. One outlier was removed in the analysis.

Since more sprouting was observed according to the vessel length marker, we had expected that the lumen surface area of the two-week vehicle group would be larger than that of the one-week vehicle group. One possible explanation for this result is that the majority of the tumor-induced micro vessels may have been dilated in the two-week vehicle group. Therefore, the surface area contributed by vessel segments with average diameters less than 50 and

70 μ m was less than that of the one-week vehicle group. However, when the diameter threshold was large enough to consider the most dilated micro vessels, the lumen surface area of the two-week vehicle group exceeded that of the one-week vehicle group.

Large Vessel Segment Diameter of Vehicle Groups

To further investigate dilation during tumor progression, we estimated the diameter distribution of every 3-D image in the two vehicle groups with a large sample disk (**Supplementary Methods**). The diameter histogram computation performed by applying a large sample disk overestimates the small-diameter vessel segments but provides better sensitivity for large-diameter vessel segments. The diameter distributions of vessel segments in the one-week and two-week vehicle groups are shown in the top and middle subplots (Figure 4C). The diameter population difference between the two vehicle groups is illustrated in the bottom subplot of Figure 4C. The negative population difference in the small diameter domain less than 200 μ m was consistent with the conclusions from the micro-vessel lumen surface area analyses using thresholds of 50 μ m and 70 μ m. The positive population difference above 200 μ m indicates that vasodilation also occurred in the vessel segments with large diameters. The larger the diameter, the less the dilation was observed.

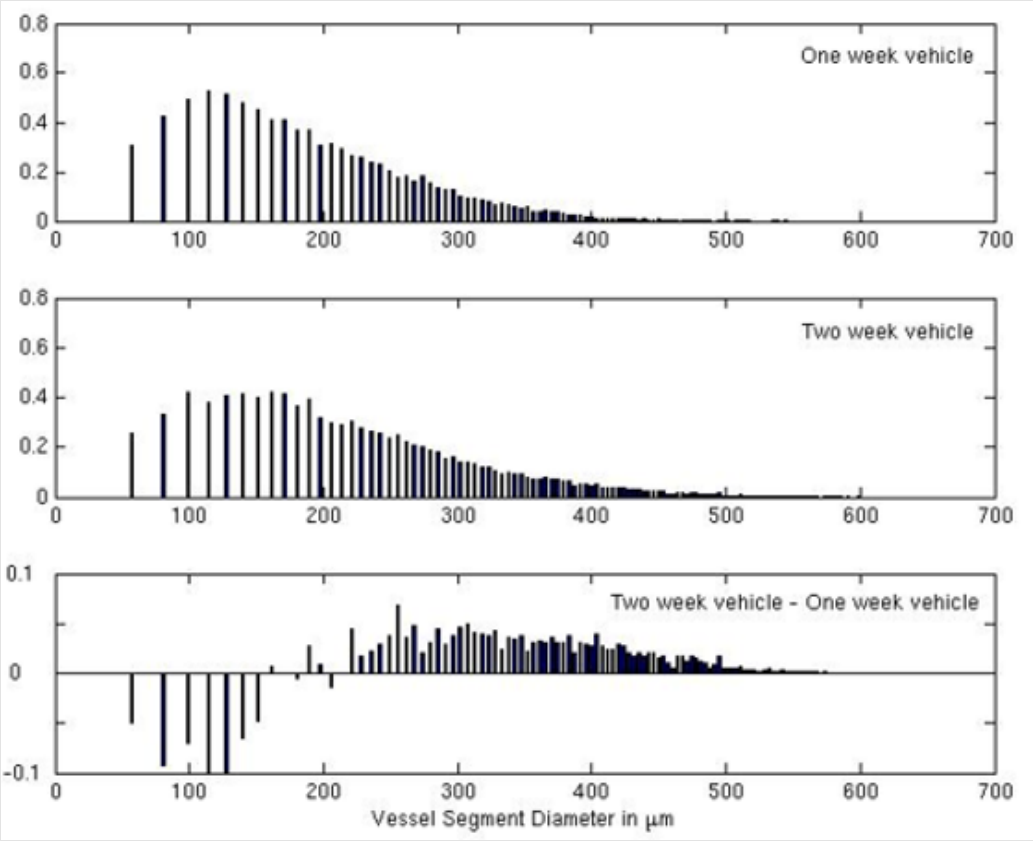

Figure 4C: Vessel segment diameter histogram of vehicle groups. Vessel segments with different diameters in the same group were accumulated and normalized by the total vessel segment number. The maximum diameter is 640 μ m. The top panel is the vessel segment diameter distribution of the one-week vehicle group; the middle panel is that of the two-week vehicle group. The diameter population contrast is illustrated on the bottom panel.

Generalized Fractal Dimension of Branch Points

Many incomparable complex patterns or signals in nature are actually driven by identical mechanisms (**Supplementary Figure 2**). Fractal dimensions can be utilized to categorize different patterns according to driving mechanisms [30-34]. Here we were interested in the fractal dimension based upon the location of the branch points in a vascular network. The formation of branch points in tumors could be related to angiogenic or anti-angiogenic mechanisms since branch points signify the diversion of nutrient transport in the circulatory network. The average fractal dimension, D0 (q = 0), of the Sutent-treated group at one week was similar to that of the Sutent-treated group at two weeks (Figure 4D). Similarly, the two vehicle groups shared approximately the same average fractal dimension D0. The median D0 of the two vehicle groups deviated from those of the two Sutent-treated groups (Figure 4D). The standard deviations of the fractal dimension were related to the number of branch points [35]. The sparse Sutent-treated vascular networks had fewer branch points available, which contributed to the higher standard deviations.

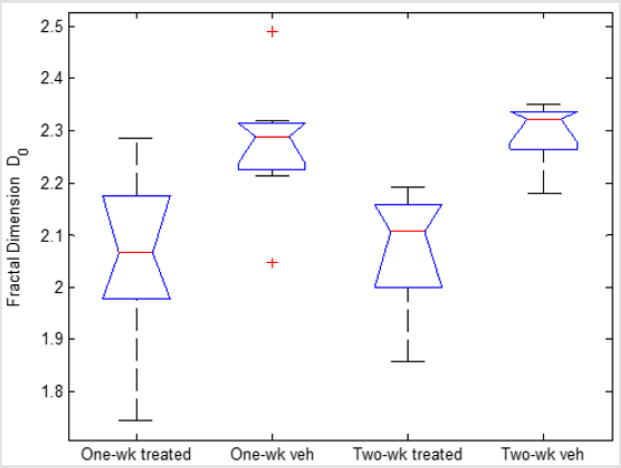

Figure 4D: Boxplot of Fractal Dimension (D0). Box and Whisker plots are used to calculate the median and variability of fractal dimension (D0) of four groups. All conventions and the symbol definition are identical to Figure 4A. The notches of Sutent-treated groups do not lie over the notches of vehicle groups. This suggests that the true median difference between the Sutent-treated groups and the vehicle groups is with 95% confidence.

Discussion

We used contrast-enhanced μ CT imaging to reveal detailed 3-D heterogeneous microvascular structure in tumors and developed imaging markers to determine different morphological aspects of the entire tumor vascular network as well as to define vascular normalization due to anti-angiogenic therapy. The observations revealed by the imaging markers were consistent with previous studies and provide a new awareness regarding tumor-induced angiogenesis. The vessel length imaging marker showed the pathological angiogenesis suppression in the tumor after one week and two-week Sutent regimens. The tortuosity marker together with the vessel length marker revealed that Sutent not only arrested angiogenesis but also normalized the tortuosity of the entire tumor vascular network. Sutent also reduced the vascular volume and the micro-vessel lumen surface area. The deviation of the mean fractal dimension indicated that the anti-angiogenic mechanism induced by Sutent was different from the angiogenic mechanism in the vehicle group. It is possible that the anti-angiogenic normalization mechanisms of different therapeutic treatments may not be the same, and the fractal dimension calculation may be able to differentiate them.

Clear normalization phenomena were shown by the imaging markers after anti-angiogenic administration; however, the progression of Sutent anti-angiogenic efficacy between the one-week and two-week regimens was difficult to determine. The comparable results from the imaging markers might suggest no significant benefit from two-week-long Sutent administration in this study. However, considering the ongoing tumor-induced angiogenesis in the tumor, two-week-long Sutent administration might still be beneficial. The 3-D imaging markers also provide insights as to how the tumor-induced vasculature changes from one week to two weeks. The vessel length, tortuosity, and vascular volume markers suggest that angiogenesis progressed from week one to week two. In contrast to our intuition and the above observation, the micro-vessel lumen surface area of the two-week vehicle group was less than that of the one-week vehicle group when considering vessel segments with diameters less than 70 μ m. Further micro-vessel sprouting in the two-week vehicle group was illustrated by the vessel length distribution.

When the larger diameter threshold (107 μ m) was applied, the lumen surface area became larger than that of the one-week vehicle group. This counterintuitive observation can be explained by vessel dilation during tumor progression, which explains the contrasting observations revealed by the lumen surface area marker and the vessel length/vascular volume markers. The results of this study also suggest that micro-vessel dilation after two weeks was more intense than after one week. Dilation in the large vessel realm was also observed. This indicates that tumor-induced angiogenesis remodels the whole vasculature in tumors and suggests that sprouting and dilation mechanisms alternatively dominate at different stages. It is tempting to speculate that tumor-induced angiogenesis is a damped cycle of sprouting and dilation mechanisms. When dilation following sprouting cannot satisfy the demand from tumor cells, another excessive sprouting cycle begins. Tumor-induced angiogenesis also triggers the dilation of large-vessel segments to compensate for the growth of micro vessels. However, how the vessel dilation signal propagates from micro vessels to upstream large vessel segments is unknown.

Angiogenesis is essential not only in cancer but also in other diseases. Unlike conventional micro-vessel density parameters from 2-D microscopy images of local tissue, our 3-D imaging markers consider the entire vasculature and supply more comprehensive analyses on vascular remodeling during tumor progression and in response to anti-angiogenic therapy. Micro-vessel density can be used as a prognostic marker, not as an efficacy marker for anti-angiogenic treatments [36,37]. Although many imaging markers in this study could be associated with functions of vascularity, the correlation between morphological markers and functional markers should be further investigated.

Acknowledgement

We thank Dr. Yufeng Lu for the discussion and Mr. Michael Philcock of Analyze Direct for the technical support.

References

1. Alitalo K (2005) Lymphangiogenesis in development and human disease. Nature 438(7070): 946-953.
2. Baish JW, Jain RK (2000) Fractals and cancer. Cancer Res 60(14): 3683-3688.

3. Bostwick DG (2000) Prognostic factors in prostate cancer. College of American Pathologists Consensus Statement 1999. Archives of Pathology & Laboratory Medicine 124(7): 995-1000.
4. Cabebe E,Wakelee H (2006) Sunitinib: a newly approved small-molecule inhibitor of angiogenesis. Drugs Today (Barc) 42(6): 387-398.
5. Carmeliet P (2003) Angiogenesis in health and disease. Nat Med 9(6): 653-660.
6. Carmeliet P (2005) Angiogenesis in life, disease and medicine. Nature. 438(7070): 932-936.
7. Carmeliet P, Jain RK (2000) Angiogenesis in cancer and other diseases. Nature 407(6801): 249-257.
8. Carmeliet P, Tessier Lavigne M (2005) Common mechanisms of nerve and blood vessel wiring. Nature 436 193-200.
9. Demetri GD (2006) Efficacy and safety of sunitinib in patients with advanced gastrointestinal stromal tumour after failure of imatinib: a randomised controlled trial. Lancet 368(9544): 1329-1338.
10. Faivre S (2006) Safety, pharmacokinetic, and antitumor activity of SU11248, a novel oral multitarget tyrosine kinase inhibitor, in patients with cancer. J Clin Oncol 24(1): 25-35.
11. Faivre S (2007) Molecular basis for sunitinib efficacy and future clinical development. Nat Rev Drug Discov 6(9):734-45.
12. Ferrara N (2003) The biology of VEGF and its receptors. Nat Med 9(6): 669-676.
13. Folkman J (1971) Tumor angiogenesis: therapeutic implications. New England Journal of Medicine. 285(21): 1182-1186.
14. Folkman J (1990) What Is the Evidence That Tumors Are Angiogenesis Dependent? J Natl Cancer Inst 82(1): 4-7.
15. Folkman J (2007) Angiogenesis: an organizing principle for drug discovery? Nat Rev Drug Discov 6(4): 273-286.
16. Greenberg DA, Jin K (2005) From angiogenesis to neuropathology. Nature 438(7070): 954-959.
17. Hashizume H (2000) Openings between Defective Endothelial Cells Explain Tumor Vessel Leakiness. Am J Pathol 156(4): 1363-1380.
18. Hicklin DJ, Ellis LM (2005) Role of the vascular endothelial growth factor pathway in tumor growth and angiogenesis. J Clin Oncol 23(5): 1011-1027.
19. Hlatky L (2002) Clinical Application of Antiangiogenic Therapy: Micro vessel Density, What It Does and Doesn't Tell Us. J Natl Cancer Inst 94(12): 883-893.
20. Jain RK (2001) Normalizing tumor vasculature with anti-angiogenic therapy: a new paradigm for combination therapy. Nat Med 7(9): 987-989.
21. Jain RK (2003) Molecular regulation of vessel maturation. Nat Med 9(6): 685-693.
22. Jain RK (2005a) Antiangiogenic therapy for cancer: current and emerging concepts. Oncology (Williston Park). 19: 7-16.
23. Jain RK (2005b) Normalization of tumor vasculature: an emerging concept in antiangiogenic therapy. Science 307(5706): 58-62.
24. Jain RK (2006) Lessons from phase III clinical trials on anti-VEGF therapy for cancer. Nat Clin Pract Oncol. 3(1): 24-40.
25. Mayr NA (2002) Method and timing of tumor volume measurement for outcome prediction in cervical cancer using magnetic resonance imaging. International Journal of Radiation Oncology Biology Physics 52(1): 14-22.
26. McDonald DM, Choyke PL (2003) Imaging of angiogenesis: from microscope to clinic. Nat Med 9(6): 713-725.
27. Miller TR, Grigsby PW (2002) Measurement of tumor volume by PET to evaluate prognosis in patients with advanced cervical cancer treated by radiation therapy. International Journal of Radiation Oncology Biology Physics. 53(2): 353-359.
28. Motzer RJ (2006a) Activity of SU11248, a Multitargeted Inhibitor of Vascular Endothelial Growth Factor Receptor and Platelet-Derived Growth Factor Receptor, in Patients with Metastatic Renal Cell Carcinoma. J Clin Oncol 24(1): 16-24.
29. Motzer RJ (2006b) Sunitinib in Patients with Metastatic Renal Cell Carcinoma. JAMA 295(21): 2516-2524.
30. Nagy JA (2002) VEGF-A induces angiogenesis, arteriogenesis, lymphangiogenesis, and vascular malformations. Cold Spring Harb Symp Quant Biol 67: 227-237.
31. Richardson TP (2001) Polymeric system for dual growth factor delivery. Nat Biotechnol 19(11): 1029-1034.
32. Sakamoto KM (2004) Su-11248 Sugen. Curr Opin Investig Drugs 5(12): 1329-1339.
33. Teicher BA (1996) A systems approach to cancer therapy. (Antioncogenics + standard cytotoxics-->mechanism(s) of interaction). Cancer Metastasis Rev. 15(2): 247-272.
34. Wan SY (2002) Multi-generational analysis and visualization of the vascular tree in 3D micro-CT images. Comput Biol Med 32(2): 55-71.
35. Wang J, Lee C (1995) Fractal characterization of an earthquake sequence. Physica A 221(1-3): 152-158.
36. Wang J, Lee C (1996) Multifractal Measures of Earthquakes in West Taiwan. PURE APPL GEOPHYS. 146: 131-145.
37. Watanabe H (2003) Tumor response to chemotherapy: The validity and reproducibility of RECIST guidelines in NSCLC patients. Cancer Science. 94(11): 1015-1020.

ISSN: 2574-1241

DOI: 10.26717/BJSTR.2020.24.004054

Chung-Wein Lee. Biomed J Sci & Tech Res